ACS OMEGA

http://pubs.acs.org/journal/acsodf

Article

Enhanced Sound Absorption Properties of Ceramics with Graphene Oxide Composites

Chao He, Bin Du,* Juan Ma, Hao Xiong, Junjie Qian, Mei Cai, and Anze Shui*

Cite This: *ACS Omega* 2021, 6, 34242−34249

Read Online

ACCESS | Metrics & More | Article Recommendations

ABSTRACT: Noise pollution is acknowledged as the main environmental problem and is as harmful to human physical and mental health as water and air pollution. However, the acoustic properties of traditional sound absorption materials in low frequency ranges still need to be improved. Herein, the low-frequency sound absorption coefficient of porous ceramics was further improved by coating a graphene oxide (GO) and styrene-butadiene rubber (SBR) composite film inside the porous ceramics. The improved sound absorption coefficient of the porous composite reached 30.4% in the range of 200−800 Hz, which is attributed to the enhancement of the thermal viscous effect and the extension of the dissipation mechanism. Predictably, designing the morphology of three-dimensional interconnected porous structures on the microscale is comparatively useful for developing a porous sound absorbing material effective in middle- and low-frequency noise.

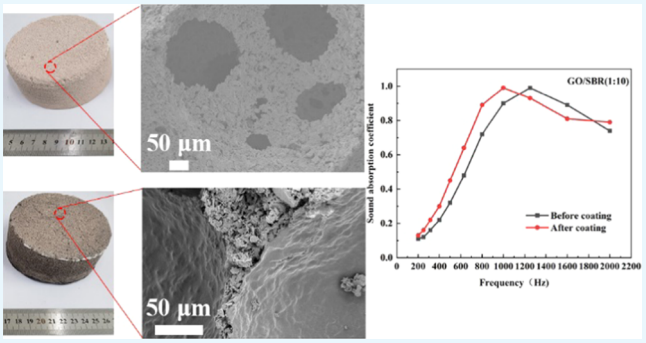

1. INTRODUCTION

Environmental noise is known to be a huge threat to public physical and psychological health.[1,2] Low- and medium-frequency noise, such as traffic and neighborhood noise, is omnipresent in daily life. Thus, the demand for acoustic absorbing materials has become urgent over the past few years. In general, most traditional sound absorbing materials, including polymer foams, porous ceramics, and metal foams, exhibit poor sound absorption performance in low and middle frequency ranges.[3−6] Some researchers enhanced the sound absorption effect of porous materials at relatively low frequencies to a certain extent by adjusting the pore structure.[7,8] However, the effect is very limited. To solve the challenging issue, researchers have already attempted to improve the properties by incorporating other materials. Carbon materials are popular fillers for porous sound absorbing materials due to their large specific surface area and excellent physical properties.[9−17] Oh et al. well arranged graphene oxide layers in a polymer foam by simple directional freezing and freeze-drying methods. The composite foam material achieved a remarkable absorbing effect at low frequencies.[10] Oh et al. also fabricated porous composite foams as acoustic absorbers by the electrostatic repulsive force of graphene oxide (GO) and activated potassium hydroxide.[13] Compared with pristine sound absorbers, the acoustic absorption coefficient of porous graphene−polyurethane foams was significantly improved. Ayub fabricated a sound absorbing material based on self-assembled interlinking GO sheets supported by a grid-type melamine framework.[16] The prepared stratified structure composite material exhibited ∼72.7% enhancement at 500 Hz compared with the melamine foam. After introducing graphene into the matrix, not only were the viscous and thermal effects improved but also the material damping effect, which plays an important role at the interface between the solid and the fluid and also converts sound energy into heat energy. Due to the material damping effect, the impact of a sound pressure wave on a skeleton structure can consume energy via a flexible motion of the porous framework.[18]

In our previous work, we prepared porous ceramics with hierarchical porous structures containing nano- and micropores by the twice foaming method. The as-prepared material possessed improved sound absorption performance in a broad absorption band between 200 and 2000 Hz.[19] However, there is still room for improvement at low frequencies. Considering the excellent sound absorption performance of the composite material and the superior dispersion and high specific surface area of GO, we tried to extend the sound absorption performance by coating a GO/styrene-butadiene rubber (SBR) film onto porous ceramics. Herein, homogeneous

Received: June 27, 2021
Accepted: November 30, 2021
Published: December 10, 2021

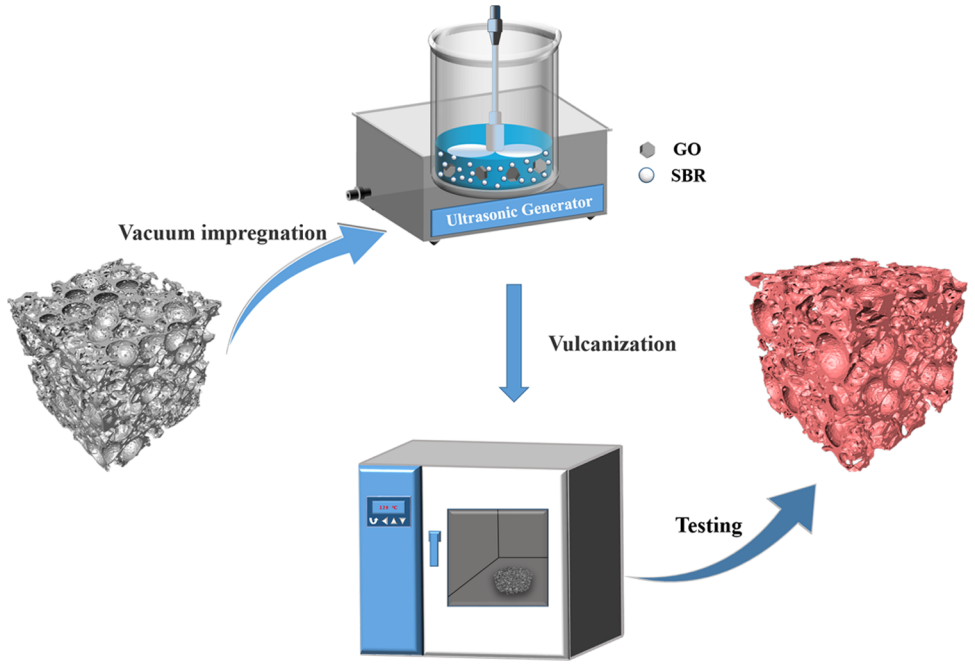

Figure 1. Schematic diagram of the synthesized GO-SBR structure in the porous ceramic skeleton.

suspensions are obtained by ultrasonication and stirring, and then GO/SBR composites were introduced by vacuum impregnation and atmospheric vulcanization to optimize the internal pore structure of the porous ceramics. Subsequently, a series of tests were performed to investigate the sound absorption performance of the porous composite materials.

2. EXPERIMENTAL SECTION

2.1. Materials. SBR latex (SBRL) with a total solid content of 48 wt % was supplied by Japan A&L Co., Ltd. GO was purchased from Knano Graphene Technology Co., Ltd. Sublimed sulfur was derived from Shanghai Aladdin Biochemical Technology Co., Ltd. Stearic acid was provided by Shanghai RichJoint Chemical Reagent Co., Ltd. 2,2′-Dibenzothiazole (DM) was supplied by Shanghai Macklin Biochemical Co., Ltd. Zinc oxide (ZnO) was obtained from Tianjin Fuchen Chemical Reagent Factory.

2.2. Preparation of Porous GO/SBR Composite Materials. Porous ceramics were used as matrices, and the detailed fabrication process was reported in our previous work.[19] The fabrication process of the porous composite materials is illustrated in Figure 1. First, different contents of GO were dispersed in deionized water with ultrasonication for 12 h. Afterward, styrene-butadiene rubber latex (SBRL) and vulcanized aqueous suspension (sublimed sulfur, DM, stearic acid, and ZnO) were dispersed in deionized water successively under intense stirring for 4 h. Then, SRRL and vulcanized aqueous suspension were mixed sequentially with the GO suspension under mechanical stirring at 650 rpm for 48 h, intermittently accompanied by water bath sonication. Subsequently, the suspension was stirred vigorously (20 000 rpm) using a high-speed disperser for 30 min. Afterward, the resulting homogeneous mixture was poured into a 2000 mL beaker with the porous ceramic matrix and then placed in vacuum for 1 h. Finally, the GO/SBR-impregnated porous ceramic matrix was vulcanized in an oven at 120 °C for 2 h and 90 °C for 12 h to obtain cross-linked GO/SBR composites. The formulae of the vulcanizing additives are SBR 100 phr, sublimed sulfur 4 phr, ZnO 5 phr, DM 3 phr, and stearic acid 1.5 phr. For all of the composites, a numerical ratio was placed after each abbreviation to denote the GO content.

2.3. Characterization. The open porosity of the sintered porous ceramic matrices was determined by Archimedes' method according to GB_1996-80. The microstructure of the sound absorbing porous materials was observed by scanning electron microscopy (SEM, Nova NanoSEM 430, the Netherlands). The sound absorption coefficient over a frequency range of 200−2000 Hz was measured using the standing wave ratio method in standing wave tubes (JTZB, JT Technology, China) according to ISO 10534-1:1996. The sound absorption coefficient α is calculated by eq 1

$$\alpha = \frac{4 \times 10^{\Delta L/20}}{(1 + 10^{\Delta L/20})^2} \quad (1)$$

where ΔL represents the difference between the maximum and minimum sound pressures. The samples are 28 mm thick and 100 mm in diameter. Each frequency was measured three times and the average value was taken as the sound absorption coefficient of the sample at that frequency. Fourier transform infrared spectroscopy (FT-IR) was performed using a transform infrared spectrometer (Nicolet iS50, Thermofisher Scientific). Thermogravimetric analysis (TGA) was studied on a Netzsch TG209F1 apparatus with a heating rate of 10 °C/min in a nitrogen atmosphere. X-ray diffraction (XRD) patterns of the samples were analyzed using an X-ray diffractometer (XRD, X'PertPro, PANalytical, Holland) with Cu Kα radiation. Raman spectroscopy was conducted using a LabRAM spectrometer (Horiba, LabRAM HR Evolution, France) with a 632 nm laser. Thermal conductivity was determined using a Hot Disk 2500 thermal constant analyzer (Hot Disk Inc., Sweden) with a transient plane source method. The well-dispersed GO sheets were characterized by atomic force microscopy (AFM, Multimode 8, Bruker).

https://doi.org/10.1021/acsomega.1c03362
ACS Omega 2021, 6, 34242−34249

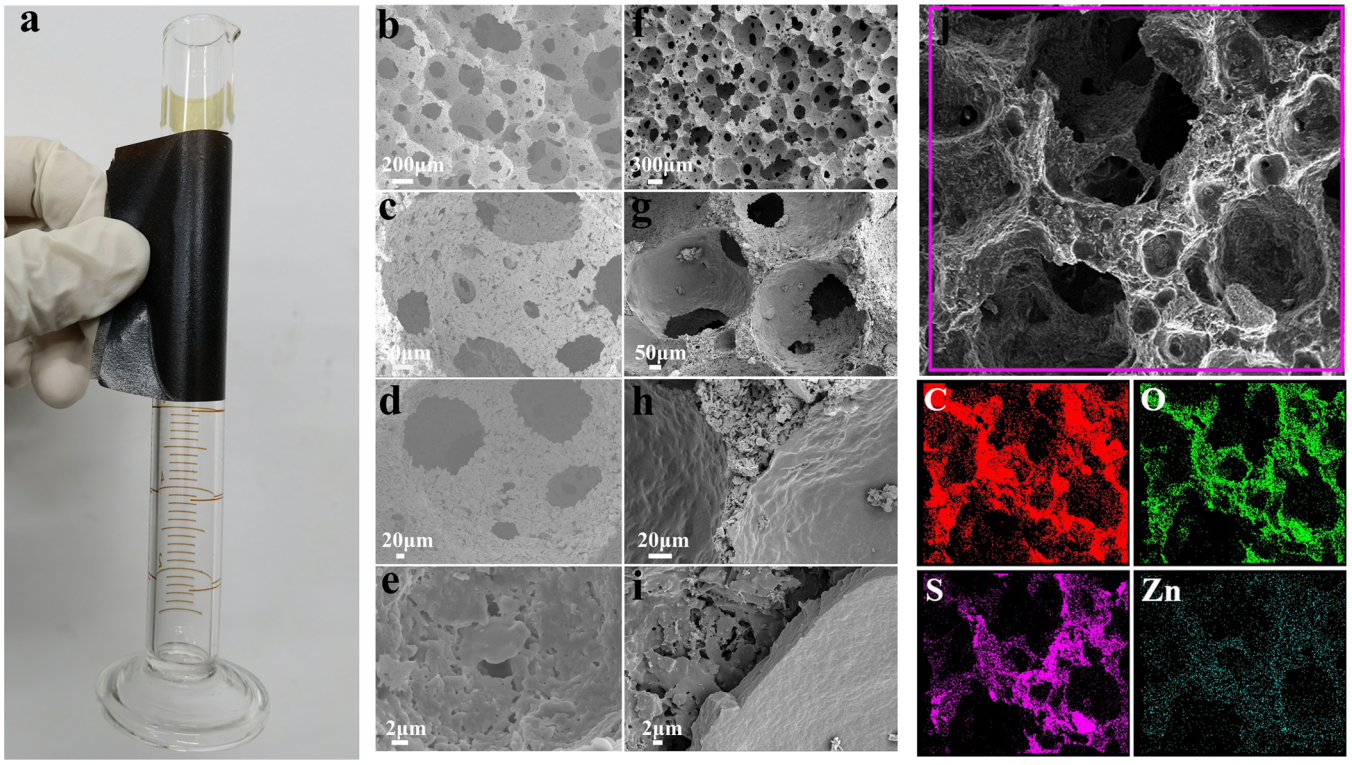

Figure 2. (a) Photograph of the GO/SBR composite film. Scanning electron micrographs of the as-obtained samples under different magnifications: (b–e) original porous ceramic matrix and (f–i) the GO/SBR (1:10) film covering the inner pore wall in the porous ceramic matrix. (j) EDS mappings of the composite material.

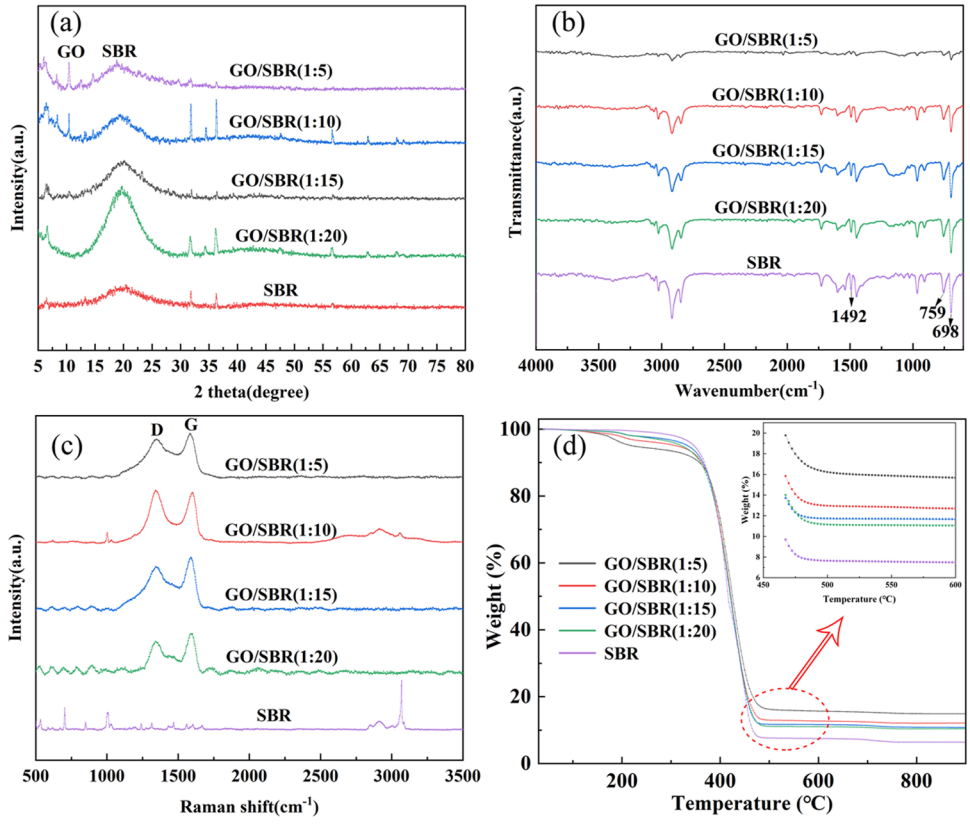

Figure 3. (a) XRD patterns, (b) FT-IR spectra, (c) Raman spectra, and (d) TGA curves of GO/SBR composite films with different contents of GO.

https://doi.org/10.1021/acsomega.1c03362
ACS Omega 2021, 6, 34242–34249

3. RESULTS AND DISCUSSION

Figure 2a shows the film photograph of GO and SBR homogenized suspensions prepared in Petri dishes by the vulcanization method. Obviously, the film possesses certain flexibility and strength. The typical structures of the raw porous ceramics before and after the formation of the GO/SBR (1:10) composite film are presented in Figure 2b−i. The raw porous ceramics with pore sizes from tens of nanometers to a few millimeters and apparent porosity in the range of 85−90% show an interconnected skeleton structure.[19] High porosity and connectivity are conducive to the incidence of sound waves, facilitating the transmission of sound waves. By vacuum impregnation and vulcanization, the GO/SBR composite and the raw porous ceramic were combined efficiently. As shown in Figure 2g,h, a thin composite film was tightly coated on the ceramic skeleton. Meanwhile, some small pores were observed below these dense films by comparing Figure 2e,i.

From Figure 2j, it can be observed that carbon, oxygen, sulfur, and zinc elements are uniformly dispersed, indicating that the GO/SBR suspensions and the vulcanizing additive are dispersed uniformly on the pore wall. The homogeneous dispersion of the mixture is the basis for the uniform combination of GO/SBR and porous ceramics and ensures that the porous GO/SBR composite materials obtain stable properties.

According to the X-ray diffraction patterns of SBR and the GO/SBR composite films shown in Figure 3a, all samples display an SBR matrix diffuse peak at 20.5° due to its amorphous structure. There is a sharp peak at 2θ = 11.0° for GO and it can only be observed at the high contents of GO (>1/15). The peaks at 2θ values of 31.7 and 36.3° are related to the (100) and (101) diffraction peaks of zinc oxide, respectively. The change of the diffraction peak of SBR, GO, and zinc oxide is similar to the previous research.[20,21] The FT-IR spectra of GO/SBR composite films are illustrated in Figure 3b. The peak at around 1492 cm^{-1} accord with the vibration of the benzene ring skeleton in the styrene unit. The peaks at around 759 and 698 cm^{-1} conform to the bending vibration of the replaced hydrogen on the benzene ring plane. The results further confirm that GO and SBR are successfully fabricated into the composite.[22] Furthermore, the Raman spectroscopy of the structural integrity of GO/SBR films was also performed. Due to its amorphous structure, SBR shows two small wide bands near 1000 and 2910 cm^{-1}, corresponding to symmetric ring breathing and CH_2 asymmetric stretching,[23,24] respectively, as illustrated in Figure 3c. After introducing GO, two conspicuous characteristic peaks near 1347 and 1585 cm^{-1} correspond to the D (defects and disorder) and G (graphitic) bands of GO, respectively.[25−27]

The thermogravimetric analysis (TGA) curves of the GO/SBR composites can be observed in Figure 3d. As noticeable from the TGA curves of GO/SBR, all GO/SBR composites present a similar degradation temperature of 357 ± 3 °C in nitrogen. Due to the limited amount of GO in our composites, the thermal stability of the GO/SBR composites is not affected. The result is similar to those of GE/SBR[22] nanocomposites and GO/NR nanocomposites.[28] The residual amounts at 700 °C are 7.1, 10.7, 11.4, 12.4, and 15.4%, which are well correlated with the GO filler content.

The thermal conductivity of the raw porous ceramics is 0.101 ± 0.005 W/mK. After using GO/SBR, the enhancement effect of thermal conductivity is proportional to the mass fraction of GO, as shown in Figure 4. However, due to the interface thermal resistance of the GO/SBR interface and the effect of vacancy

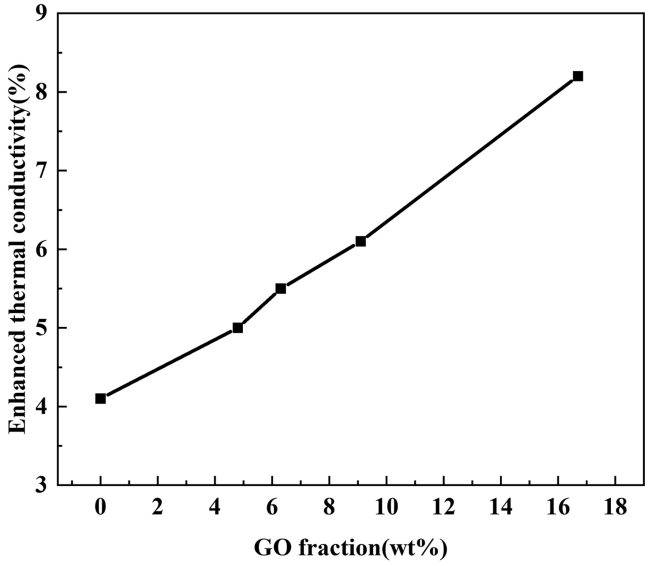

Figure 4. Thermal conductivity of the composite with different contents of GO.

defects on the intrinsic thermal conductivity of GO, the increase of the thermal conductivity of the porous materials after coating is not obvious.[29] Similar results for NR/GE composites were reported.[30] This will not affect the use of sound absorbing materials as building materials.

Figure 5 displays the sound absorption coefficient curves of all samples. With the increase of the GO content, the sound absorption coefficient gradually increases, especially in the range of 200−800 Hz, as shown in Table 1. Furthermore, the maximum of the sound absorption curve moved toward the low frequency. When the mixing amounts of GO and SBR are in a ratio of 1:10, the improvement of sound absorption performance reached the maximum. When the porous ceramic was coated with the pure SBR latex with the same solid content (2 wt %), the sound absorption coefficient decreases instead. This is because the lack of a micron-size GO network connection will make the SBR particles further move into the internal pores of the porous ceramic skeleton;[31] thus, no film was formed on the surface of the inner cell wall and many connected nanopores were undoubtedly blocked, as shown in Figure 6.

It is known that low-frequency sound has stronger penetrating power than medium- and high-frequency sound. The mass density law (eq 2) can in part explain this phenomenon.

$$\mathrm{STL}(\theta) = 10\log_{10}\left[1 + \left(\frac{\pi \times f \times \rho \times d}{\rho_0 \times c}\cos\theta\right)^2\right] \quad (2)$$

Here, f denotes the acoustic frequency; ρ_0 and c are the mass density of air and the sound velocity in air, respectively. $\mathrm{STL}(\theta)$ represents the loss of sound waves with incident angle θ when passing through a material. The sound transmission loss is inversely proportional to the product of the thickness d, the mass density ρ of the material, and the frequency f. Therefore, when the film was coated on the porous ceramic, the incidence of low-frequency acoustic waves onto the porous material was not significantly affected. Moreover, thermal and viscous losses will lead to sound attenuation when sound propagates in narrow pores. Specifically, the loss occurs in the acoustic thermal boundary layer and the viscous boundary layer near the pore wall. The length δ

https://doi.org/10.1021/acsomega.1c03362
ACS Omega 2021, 6, 34242−34249

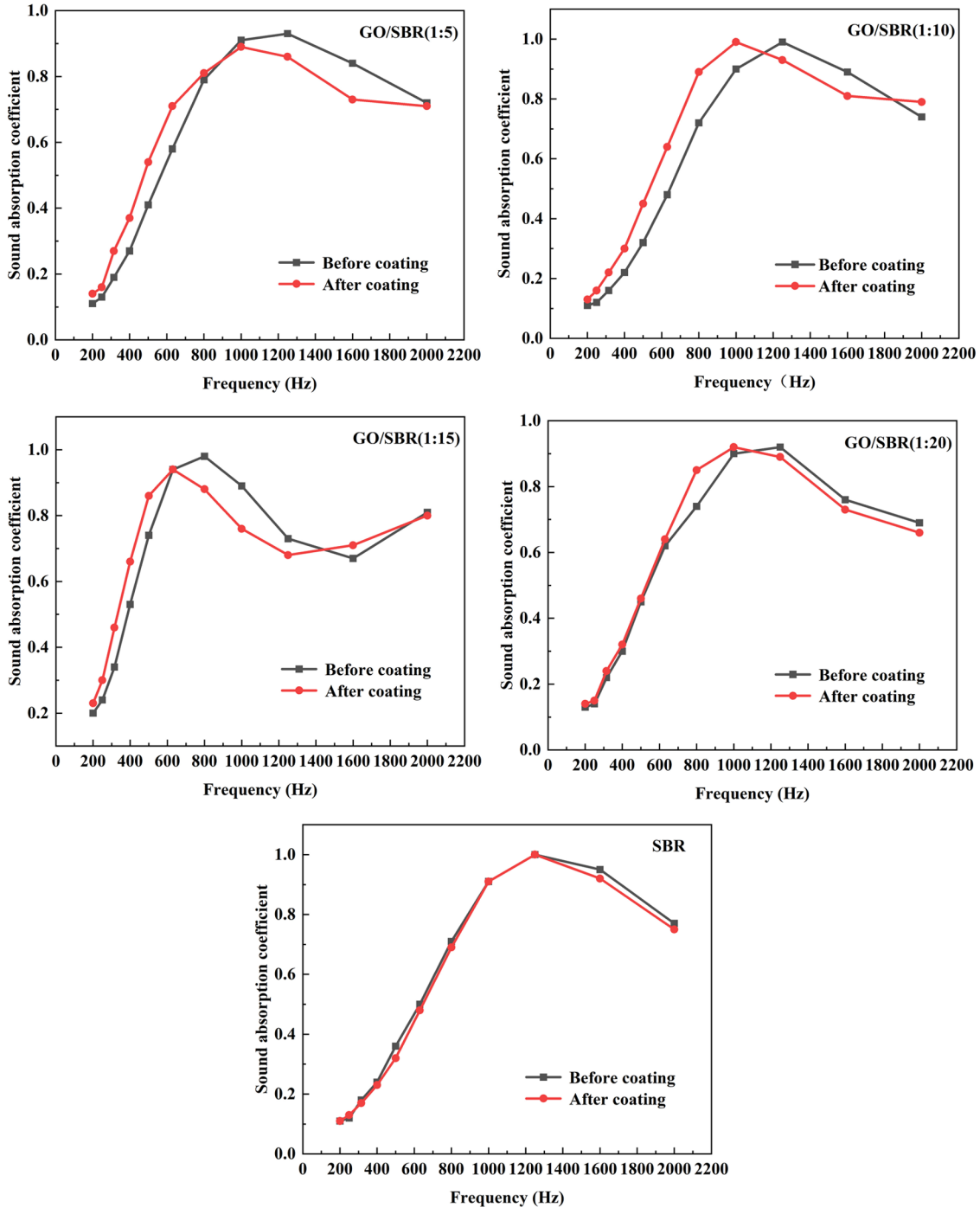

Figure 5. Sound absorption coefficient of the composite porous materials with different contents of GO.

Table 1. Comparison of the Sound Absorption Performance of Porous Materials before and after Coating

sample	frequency equivalent to the maximum sound absorption coefficient before coating (Hz)	frequency equivalent to the maximum sound absorption coefficient after coating (Hz)	improvement rate of average sound absorption before 800 Hz (%)	improvement rate of the noise reduction coefficient from 200 to 2000 Hz (%)
GO/SBR (1:5)	1250	1000	21.2	7.4
GO/SBR (1:10)	1250	1000	30.4	15.4
GO/SBR (1:15)	800	630	8.7	1.5
GO/SBR (1:20)	1250	1000	8.1	0.4
SBR	1250	1250	−4.1	−2.3

https://doi.org/10.1021/acsomega.1c03362
ACS Omega 2021, 6, 34242−34249

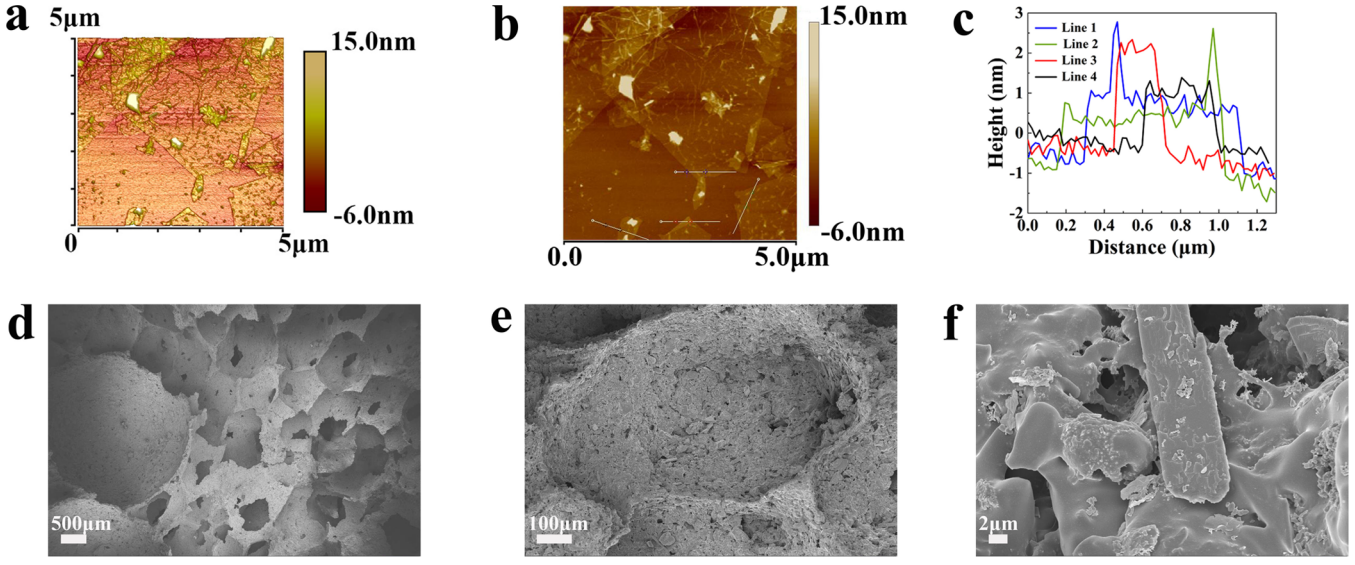

Figure 6. (a) Three-dimensional AFM images of the GO aqueous solution; (b) 2D morphology of the GO aqueous solution; (c) height statistical line diagram; and (d–f) SEM images of the composite porous materials with pure SBR.

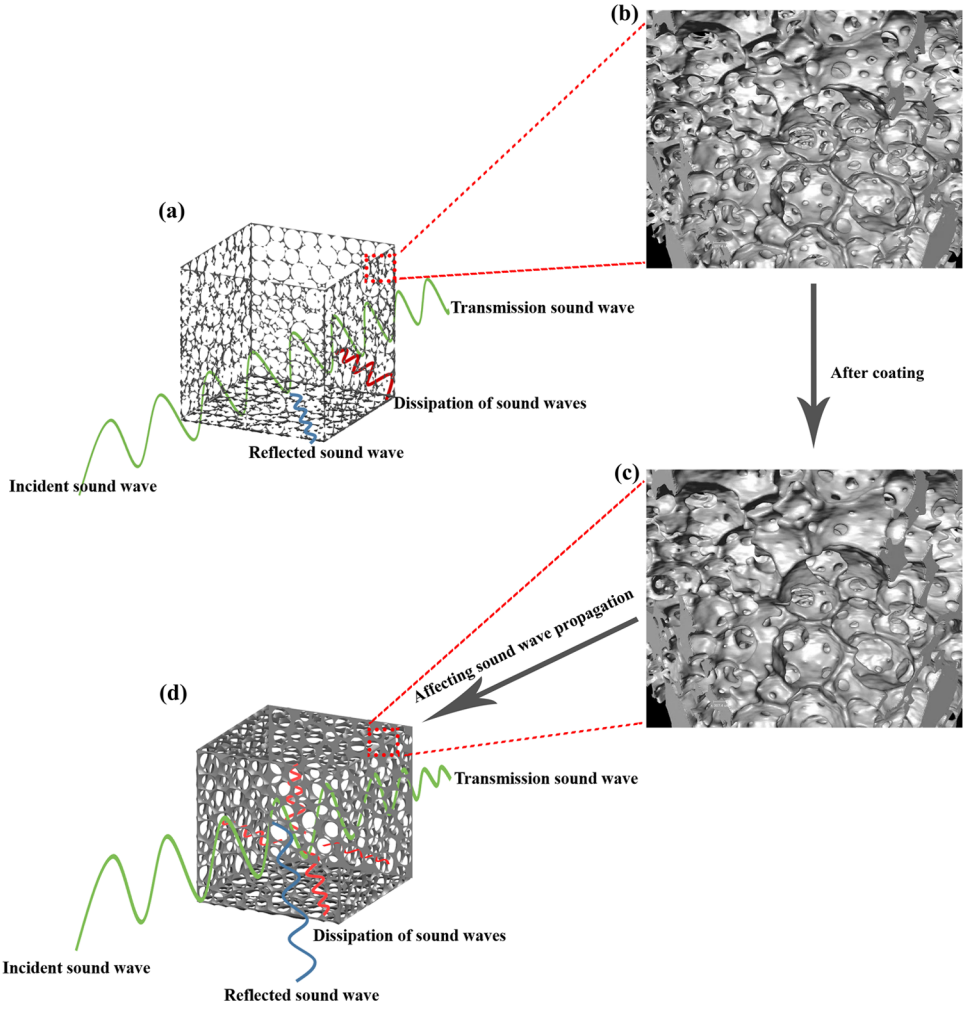

Figure 7. (a, b) Schematics of wave propagation through porous ceramics before and after GO impregnation, (c) 3D representative volume element of the raw porous ceramics, and (d) simulation picture of the dilated internal skeleton structure made by adding pixels.

https://doi.org/10.1021/acsomega.1c03362
ACS Omega 2021, 6, 34242−34249

$$\delta = \left(\frac{2\eta}{\omega\rho_0}\right)^{1/2} \quad (3)$$

denotes the viscous boundary layer thickness. This thickness approaches the length of the layer of air near the surface of the pore wall with the considerable viscous force generated by the motionless skeleton. Meanwhile, this viscous force greatly affects the velocity distribution.[32] Similarly, thermal boundary layer thickness δ' is given by

$$\delta' = \left(\frac{2\kappa}{\omega\rho_0 C_P}\right)^{1/2} \quad (4)$$

Here, η denotes the shear viscosity; κ is the thermal conductivity; ω and ρ_0 are the angular frequency ($\omega = 2\pi f$, where f is the sound frequency) of the acoustic wave and air density, respectively; and C_P is the specific heat per unit mass at constant pressure. When the pore size is up to a certain range,

$$R \ll \left(\frac{\eta}{\omega\rho_0}\right)^{1/2} \quad (5)$$

the influence of the viscous forces and thermal effects is significant and nonnegligible everywhere in the pore. Therefore, when the composite film divided the connected pore structure and produced more boundaries, the transmission path of sound waves in the porous materials became more tortuous, causing numerous acoustic reflections and friction of the air flow, resulting in dissipating more incident sound waves and moving the sound absorption curves toward lower frequencies (Figure 7).[12,13,15] In addition, multiple absorption mechanisms can generate the inherently fine damping properties of the viscoelastic SBR substrate and the dissipation of acoustic waves between the graphene oxide layers and the GO/SBR interfaces by friction and sliding.[11] Moreover, the vibration of the GO/SBR film consumes energy as well. However, part of middle- and high-frequency sound waves were directly reflected by the composite film rather than transmission so that the absorption coefficients were decreased in the medium frequency (Figure 7).

4. CONCLUSIONS

In summary, an environmentally friendly and sound absorbing composite, i.e., GO/SRB film-coated porous ceramics, was designed and experimentally demonstrated. Compared to raw porous ceramics, the sound absorption coefficient of the porous composite material after coating improved 30.4% in a frequency range of 200−800 Hz and the NRC enhanced more than 15.4%. The results demonstrated that the low-frequency sound absorption coefficient can be effectively improved by introducing a flexible second-phase material into a rigid frame sound absorber to design the pore structure reasonably. Meanwhile, the sound absorber has low thermal conductivity, which might be very beneficial for building applications.

AUTHOR INFORMATION

Corresponding Authors

Bin Du − *School of Materials Science and Engineering, South China University of Technology, Guangzhou 510641, P. R. China*; Phone: +86 020 87110290; Email: dubin@scut.edu.cn

Anze Shui − *School of Materials Science and Engineering, South China University of Technology, Guangzhou 510641, P. R. China*; Phone: +86 020 87110290; Email: shuianze@scut.edu.cn

Authors

Chao He − *School of Materials Science and Engineering, South China University of Technology, Guangzhou 510641, P. R. China*; orcid.org/0000-0002-6467-6320

Juan Ma − *School of Materials Science and Engineering, South China University of Technology, Guangzhou 510641, P. R. China*

Hao Xiong − *School of Materials Science and Engineering, South China University of Technology, Guangzhou 510641, P. R. China*

Junjie Qian − *School of Materials Science and Engineering, South China University of Technology, Guangzhou 510641, P. R. China*

Mei Cai − *School of Materials Science and Engineering, South China University of Technology, Guangzhou 510641, P. R. China*

Complete contact information is available at: https://pubs.acs.org/10.1021/acsomega.1c03362

Notes

The authors declare no competing financial interest.

ACKNOWLEDGMENTS

This work was supported by the National Natural Science Foundation of China (51772102, 51972114, and 51902107), the National Natural Science Foundation of Guangdong Province (2019A1515011002 and 2019A1515011992), Guangdong YangFan Innovative & Entrepreneurial Research Team Program (2016YT03C327), China Postdoctoral Science Foundation (2018M643074 and 2019T120728), Meizhou Science and Technology Project (2019A0101021), Fundamental Research Funds for the Central Universities (2019MS002), and Zhujiang Delta Water Resources Allocation Project (CD88-GC02-2020-0012).

REFERENCES

(1) Dreger, S.; Meyer, N.; Fromme, H.; Bolte, G. Environmental noise and incident mental health problems: A prospective cohort study among school children in Germany. *Environ. Res.* **2015**, *143*, 49−54.

(2) Gan, W. Q.; Davies, H. W.; Koehoorn, M.; Brauer, M. Association of long-term exposure to community noise and traffic-related air pollution with coronary heart disease mortality. *Am. J. Epidemiol.* **2012**, *175*, 898−906.

(3) Du, Z.; Yao, D.; Xia, Y.; Zuo, K.; Yin, J.; Liang, H.; Zeng, Y.-P. Highly porous silica foams prepared via direct foaming with mixed surfactants and their sound absorption characteristics. *Ceram. Int.* **2020**, *46*, 12942−12947.

(4) Wu, G.; Li, R.; Yuan, Y.; Jiang, L.; Sun, D. Sound absorption properties of ceramic hollow sphere structures with micro-sized open cell. *Mater. Lett.* **2014**, *134*, 268−271.

(5) Liu, P. S.; Qing, H. B.; Hou, H. L. Primary investigation on sound absorption performance of highly porous titanium foams. *Mater. Des.* **2015**, *85*, 275−281.

(6) Yang, X.; Peng, K.; Shen, X.; Zhang, X.; Bai, P.; Xu, P. Geometrical and Dimensional Optimization of Sound Absorbing Porous Copper with Cavity. *Mater. Des.* **2017**, *131*, 297−306.

(7) Chen, J. H.; Liu, P. S.; Sun, J. X. Sound absorption performance of a lightweight ceramic foam. *Ceram. Int.* **2020**, *46*, 22699−22708.

(8) Liu, P. S.; Ma, X. M. Property relations based on the octahedral structure model with body-centered cubic mode for porous metal foams. *Mater. Des.* **2020**, *188*, No. 108413.
(9) Wu, Y.; Sun, X.; Wu, W.; Liu, X.; Lin, X.; Shen, X.; Wang, Z.; Li, R. K. Y.; Yang, Z.; Lau, K.-T.; Kim, J.-K. Graphene foam/carbon nanotube/poly(dimethyl siloxane) composites as excellent sound absorber. *Composites, Part A* **2017**, *102*, 391−399.
(10) Oh, J. H.; Kim, J.; Lee, H.; Kang, Y.; Oh, I. K. Directionally Antagonistic Graphene Oxide-Polyurethane Hybrid Aerogel as a Sound Absorber. *ACS Appl. Mater. Interfaces* **2018**, *10*, 22650−22660.
(11) Liu, L.; Chen, Y.; Liu, H.; Rehman, H. U.; Chen, C.; Kang, H.; Li, H. A graphene oxide and functionalized carbon nanotube based semi-open cellular network for sound absorption. *Soft Matter* **2019**, *15*, 2269−2276.
(12) Kim, J. M.; Kim, D. H.; Kim, J.; Lee, J. W.; Kim, W. N. Effect of graphene on the sound damping properties of flexible polyurethane foams. *Macromol. Res.* **2017**, *25*, 190−196.
(13) Oh, J.-H.; Lee, H. R.; Umrao, S.; Kang, Y. J.; Oh, I.-K. Self-aligned and hierarchically porous graphene-polyurethane foams for acoustic wave absorption. *Carbon* **2019**, *147*, 510−518.
(14) Oh, J.-H.; Kim, J.-S.; Nguyen, V. H.; Oh, I.-K. Auxetic graphene oxide-porous foam for acoustic wave and shock energy dissipation. *Composites, Part B* **2020**, *186*, No. 107817.
(15) Lee, J.; Jung, I. Tuning sound absorbing properties of open cell polyurethane foam by impregnating graphene oxide. *Appl. Acoust.* **2019**, *151*, 10−21.
(16) Nine, M. J.; Ayub, M.; Zander, A. C.; Tran, D. N. H.; Cazzolato, B. S.; Losic, D. Graphene Oxide-Based Lamella Network for Enhanced Sound Absorption. *Adv. Funct. Mater.* **2017**, *27*, No. 1703820.
(17) Huang, Y.; Wan, C. Controllable fabrication and multifunctional applications of graphene/ceramic composites. *J. Adv. Ceram.* **2020**, *9*, 271−291.
(18) Rahimabady, M.; Statharas, E. C.; Yao, K.; Sharifzadeh Mirshekarloo, M.; Chen, S.; Tay, F. E. H. Hybrid local piezoelectric and conductive functions for high performance airborne sound absorption. *Appl. Phys. Lett.* **2017**, *111*, No. 241601.
(19) He, C.; Du, B.; Qian, J.; Wang, X.; Luo, B.; Shui, A. Synthesis of macroporous ceramic with enhanced sound absorption capability in low and medium frequency. *Ceram. Int.* **2020**, *46*, 17917−17922.
(20) Xing, W.; Tang, M.; Wu, J.; Huang, G.; Li, H.; Lei, Z.; Fu, X.; Li, H. Multifunctional properties of graphene/rubber nanocomposites fabricated by a modified latex compounding method. *Compos. Sci. Technol.* **2014**, *99*, 67−74.
(21) Bai, X.; Wan, C.; Zhang, Y.; Zhai, Y. Reinforcement of hydrogenated carboxylated nitrile−butadiene rubber with exfoliated graphene oxide. *Carbon* **2011**, *49*, 1608−1613.
(22) Li, Y.; Xu, F.; Lin, Z.; Sun, X.; Peng, Q.; Yuan, Y.; Wang, S.; Yang, Z.; He, X.; Li, Y. Electrically and thermally conductive underwater acoustically absorptive graphene/rubber nanocomposites for multi-functional applications. *Nanoscale* **2017**, *9*, 14476−14485.
(23) Prasertsri, S.; Lagarde, F.; Rattanasom, N.; Sirisinha, C.; Daniel, P. Raman spectroscopy and thermal analysis of gum and silica-filled NR/SBR blends prepared from latex system. *Polym. Test.* **2013**, *32*, 852−861.
(24) Martínez-Barrera, G.; López, H.; Castaño, V. M.; Rodríguez, R. Studies on the rubber phase stability in gamma irradiated polystyrene-SBR blends by using FT-IR and Raman spectroscopy. *Radiat. Phys. Chem.* **2004**, *69*, 155−162.
(25) Dresselhaus, M. S.; Jorio, A.; Hofmann, M.; Dresselhaus, G.; Saito, R. Perspectives on carbon nanotubes and graphene Raman spectroscopy. *Nano Lett.* **2010**, *10*, 751−758.
(26) Yang, D.; Velamakanni, A.; Bozoklu, G.; Park, S.; Stoller, M.; Piner, R. D.; Stankovich, S.; Jung, I.; Field, D. A.; Ventrice, C. A.; Ruoff, R. S. Chemical analysis of graphene oxide films after heat and chemical treatments by X-ray photoelectron and Micro-Raman spectroscopy. *Carbon* **2009**, *47*, 145−152.
(27) Daniela, C. Improved Synthesis of Graphene Oxide. *ACS Nano* **2010**, *4*, 4806−4814.
(28) Matos, C. F.; Galembeck, F.; Zarbin, A. J. G. Multifunctional and environmentally friendly nanocomposites between natural rubber and graphene or graphene oxide. *Carbon* **2014**, *78*, 469−479.
(29) Luo, T.; Lloyd, J. R. Enhancement of Thermal Energy Transport Across Graphene/Graphite and Polymer Interfaces: A Molecular Dynamics Study. *Adv. Funct. Mater.* **2012**, *22*, 2495−2502.
(30) Zhan, Y.; Wu, J.; Xia, H.; Yan, N.; Fei, G.; Yuan, G. Dispersion and Exfoliation of Graphene in Rubber by an Ultrasonically-Assisted Latex Mixing and In situ Reduction Process. *Macromol. Mater. Eng.* **2011**, *296*, 590−602.
(31) Xing, W.; Li, H.; Huang, G.; Cai, L.-H.; Wu, J. Graphene oxide induced crosslinking and reinforcement of elastomers. *Compos. Sci. Technol.* **2017**, *144*, 223−229.
(32) Allard, J. F.; Atalla, N. Propagation of Sound in Porous Media:Modelling Sound Absorbing. In *Materials*, 2nd ed.; John Wiley & Sons, 2009; p 3.

https://doi.org/10.1021/acsomega.1c03362
ACS Omega 2021, 6, 34242−34249